Microstructure and Mechanical Properties of Dual Phase Steel Produced by Laser Powder Bed Fusion

Kerri Horvay, Chris Schade, Tom Murphy
Hoeganaes Corporation
Cinnaminson, NJ 08077

ABSTRACT

As the demand for additive manufacturing in automotive and industrial applications increases, more development work is needed to expand the range of suitable metal powders. Dual phase (DP) steels are widely used in the automotive industry due to their combination of high strength and good formability. Intercritical annealing heat treatments are used with these steels to optimize mechanical performance by producing a two-phase microstructure consisting of islands of hard martensite and a soft ferrite matrix. DP600, a popular grade used for various automotive parts, was chosen for this study to investigate the mechanical properties and microstructure of components manufactured by laser powder bed fusion (LPBF). Charpy impact testing is used to characterize the fracture behavior of the alloy and the impact energy is examined in relation to the microstructure developed during heat treatment. By using post-processing heat treatments the range of mechanical properties achievable will be shown, which provides greater flexibility to the end user by allowing one material to be utilized across various applications.

INTRODUCTION

Dual phase steels are processed by traditional thermomechanical methods and are used in various car components including floor panels, fenders, rear rails, safety cage components, roof rails, etc.[1] They have superior formability as compared to conventional steels which is beneficial for part fabrication. The microstructure of the steel typically contains a mixture of ferrite and 15-20% martensite.[2] Components made from DP sheet metal are created from steel slabs that may go through various hot and cold rolling processes to reduce its thickness, which then are passed through a continuous annealing furnace at a high temperature to intercritically anneal into the ferrite-austenite region and cooled rapidly to transform the austenite to a hard second phase (martensite or bainite).[1] The characteristics of the second phase (size, shape, distribution, etc.) are important in determining the material properties.[3] By using this material with additive manufacturing current automotive metal parts can be adapted for prototyping or new components can be developed. Because LPBF uses a different thermal profile than conventional methods where the final microstructure is controlled by factors such as the rolling processes, intercritical annealing

temperature, time at temperature and the cooling rate, thermal post-processing can be used to achieve the required material properties.[4]

The dual phase steel, DP600, is an attractive material for additive manufacturing due to the wide range of properties that can be produced by laser printing and heat treating allowing one material to meet a variety of property requirements. In previous work tensile, fatigue, and compression properties of DP600 processed by LPBF were examined, while this study also examines the impact behavior of the alloy.[5] Impact testing is a simple inexpensive test to determine the toughness of a material. Because additive manufacturing can produce complex geometries it would be economical to produce a standard test piece that could be used without machining to reduce costs and time. Using a printed sample for preliminary testing instead of machining could allow for a quicker comparison of materials for alloy development. Charpy V-notch impact testing is used to measure the toughness of a material in terms of the absorbed energy to break the specimen. The standard test sample is shown in Figure 1.

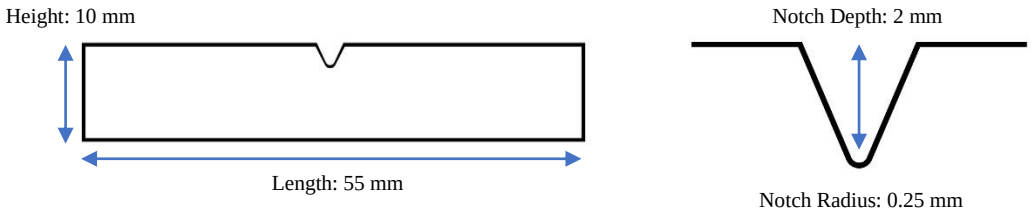

Figure 1. Diagram showing ASTM Standard E23 Charpy V-notch impact bar dimensions.

Parameters that affect the toughness include the material, microstructure, level of impurities, grain size and orientation, specimen size, notch geometry, loading rate, temperature, etc. In order to maintain a balance between toughness and strength, the microstructure needs to be manipulated. Variations in the notch will also produce variation in the impact energy. Figure 2 shows data from Table X1.1 in ASTM Standard E23.[6] As the notch depth increases the impact energy decreases. As the radius at the base of notch increases (becomes less sharp) the impact energy increases. Thus, the laser printed impact bar must be examined in comparison to a machined impact bar.

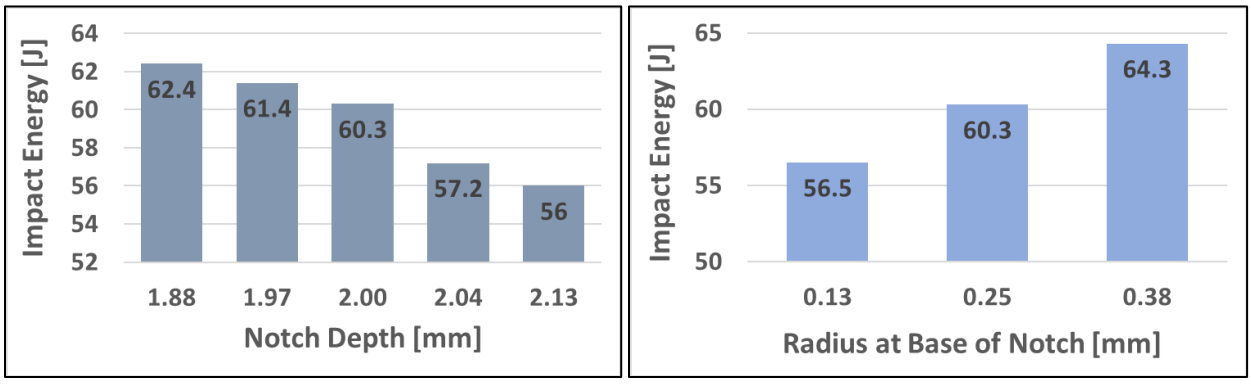

Figure 2. Graphs displaying the influence of (left) notch depth and (right) notch radius on impact energy. The data is for medium energy specimens taken from Table X1.1 in ASTM Standard E23.[6]

EXPERIMENTAL PROCEDURE

Powder Characterization

The powder used in this study was gas atomized and screened to a nominal 15-53 µm particle size that is typically used in LPBF processing. The chemical composition of the powder is listed below in Table I and meets the wrought specification for DP600.

Table I: Chemical composition of powder used in this study and wrought specification (wt.%).

Material	Carbon	Manganese	Silicon	Chromium	Iron
Wrought	0.14 max	2.00 max	1.50 max	1.00 max	Balance
Powder	0.11	1.62	0.30	<0.01	Balance

The particle size and physical properties of the powder are shown in Table II. Apparent density, tap density and flow were measured in accordance with MPIF Standards 28, 46 and 03 respectively. Scanning electron microscopy (SEM) was used to observe the powder morphology as shown in Figure 3.

Table II: DP600 powder properties.

d_{10} [µm]	d_{50} [µm]	d_{90} [µm]	Apparent Density [g/cm^3]	Tap Density [g/cm^3]	Hall Flow [sec]
16.9	33.7	56.0	3.89	5.00	17.7

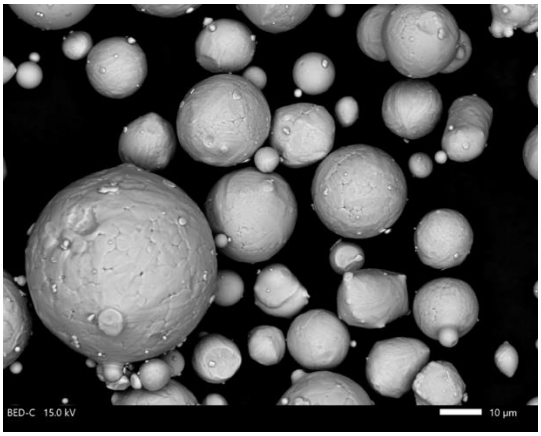

Figure 3. Morphology of gas atomized DP600 powder. SEM

LPBF Processing

An EOS M290 machine was used to make the testing specimens by melting powder layer by layer with a Yb fiber laser (400 W) within an argon filled chamber. Cubic samples (10 mm by 10 mm by 10 mm) were printed with a variety of settings to evaluate the porosity content. A constant layer thickness was used for all the samples while the laser power, hatch distance, and scanning speed were varied. Image analysis, following MPIF standard guide 69, was used to measure the porosity content of the cross-sections of the cubes perpendicular to the build direction.[7] A set of standard settings was chosen that led to a density greater than 99.0% to use as the printing parameters. Conventional flat "dogbone" tensile specimens per MPIF Standard 10 were printed in the Z direction and cut from the build plate in the as-built condition.[7] ASTM E23 Charpy V-notch samples (10 mm x 10 mm x 55 mm) as shown in Figure 1 were printed with the required notch in the Z direction as well as specimen blanks to be machined.

Charpy V-notch bars were also printed in the X direction with the required notch to observe the difference in size and shape of the notch when printing samples in different orientations on the build plate as shown in Figure 4. After printing, the samples were cut from the build plate and the sample blanks were machined to ASTM E23 specifications. A Mitutyo SJ-210 surface roughness tester was used to measure the Ra, the average surface roughness, of the impact bars. SEM was used to observe the surface of the different notch types.

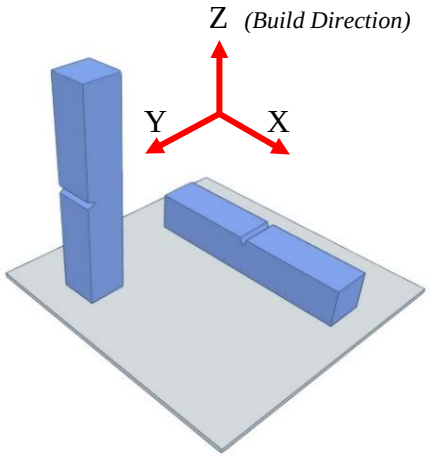

Figure 4. Diagram showing the printing direction of the Charpy V-notch bars.

Heat Treatment

Different heat treatments were used to investigate different microstructures and the corresponding mechanical properties. The cycles were chosen based on calculations made with a thermodynamic software (Thermocalc) to estimate the alloy's Ac1, the temperature where austenite begins to transform, and the Ac3, the temperature where the austenite transformation is complete. The phase diagram of DP600 grade steel by varying carbon content is shown in Figure 5.

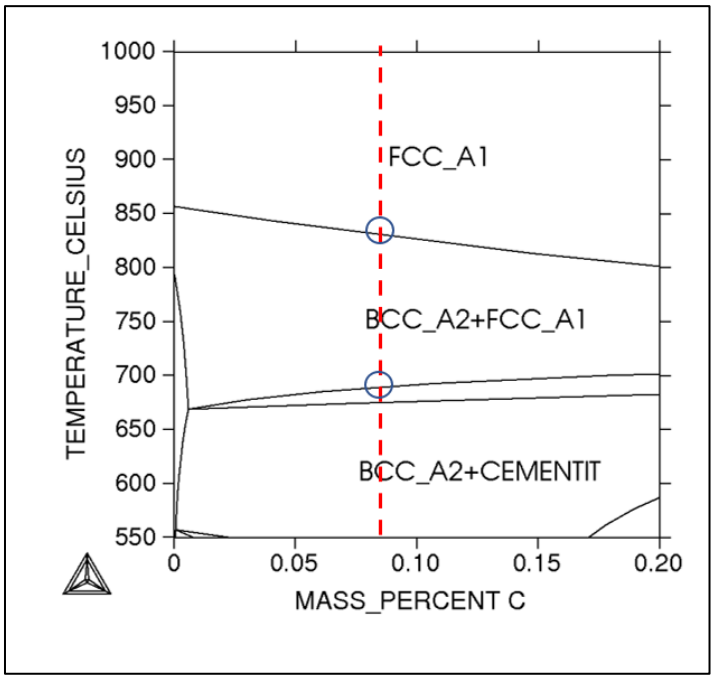

Figure 5. Phase diagram of DP600 grade steel by varying carbon content.

The red dashed line shows the phases present at equilibrium at different temperatures. The two temperatures at which red line intersects the austenite and ferrite field are the intercritical annealing temperature range. These temperatures are indicated by the blue circles. When the steel is heated in this temperature range and rapidly cooled the austenite will transform to martensite or bainite and the primary ferrite will remain.[8]

The heat treatments used in this study are shown in Table III. A batch furnace with a nitrogen atmosphere was used to heat treat the tensile bars, machined V-notch bars, and printed V-notch bars. Two intercritical annealing temperatures were chosen based on the phase diagram, 746 °C and 816 °C, to produce different proportions of ferrite and austenite. The samples were held at temperature for 1 hour and then water quenched (WQ) to transform the austenite. Samples were also austenitized at 899 °C to produce a homogeneous austenitic phase during heating and then air cooled (AC).[8] The last heat treatment was to austenitize and air cool then intercritcally anneal to produce a more uniform dual phase microstructure. Those samples were first held at 899 °C for 1 hour followed by air cooling and then heated to 746 °C for 1 hour followed by water quenching. These different heat treatments were expected to produce a range of microstructures with varying mechanical properties.

Table III: Heat treatment cycles for LPBF samples.

Heat Treatment Type	Temperature & Cooling Method
Intercritical Anneal	746 °C, water quench
Intercritical Anneal	816 °C, water quench
Austenitize	899 °C, air cool
Austenitize + Intercritical Anneal	899 °C, air cool + 746 °C, water quench

Mechanical Testing

Hardness measurements and tension testing were conducted in accordance with MPIF Standards 43 and 10 respectively. Impact testing was completed following ASTM E23 at room temperature. Metallographic testing was performed on cross-sections of the test samples that were etched with 2 vol. % nital + 4 wt.% picral. A scanning electron microscope (SEM) was used to observe the microstructure of the samples. Electron backscatter diffraction (EBSD) was used to confirm the phases present in each sample. SEM was also used to evaluate the fracture surfaces of the impact bars.

RESULTS & DISCUSSION

The notches of the impact bars were imaged to compare the differences in size and shape of the notch. Figure 6a shows the notch of the bar printed in the Z direction. It had the smallest notch depth and most irregular notch base. Figure 6b shows the notch of the bar printed in the X direction. This notch was closer to the target requirements than the Z bar. Figure 6c shows the notch of the bar that was machined. The Z and X printed notch bars did not meet the ASTM specification for Charpy V-notch bars, but the improvement seen in the X bar shows further printer parameter development and part design could produce a more consistent notch. Variations in notch geometry will influence the resulting impact energy as shown by the data in Figure 2 from ASTM E23. Based on that data as the notch depth decreases the impact energy increases and as the radius of the notch base decreases (becomes more sharp) the impact energy decreases.[9]

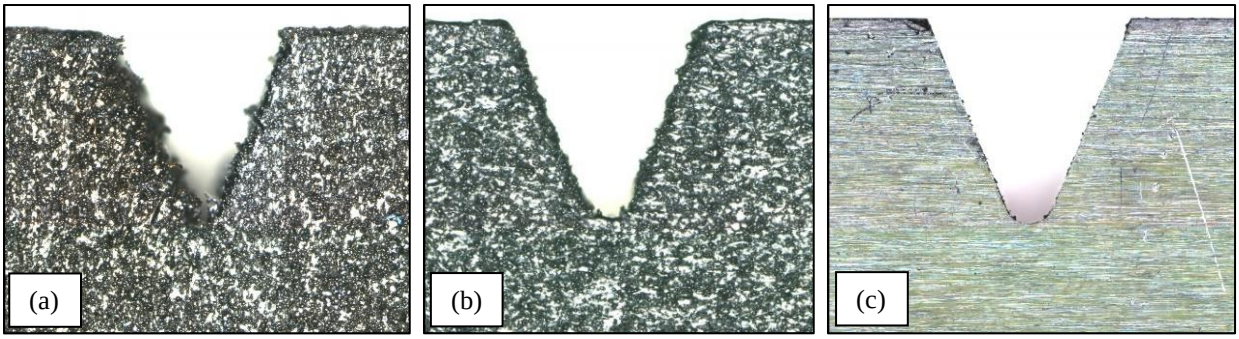

Figure 6. Images showing the resulting notch of the (a) printed Z bar, (b) printed X bar and (c) machined bar.

Images of the top face of the impact bars were taken as well as SEM images of the interior of the notch as shown in Figure 7. Partially melted powder particles in the notch of the Z bar are observed as compared to the smooth surface finish of the machined bar. To achieve a better surface finish optimized print parameters and part design may be needed to reach targeted part dimensions.[4]

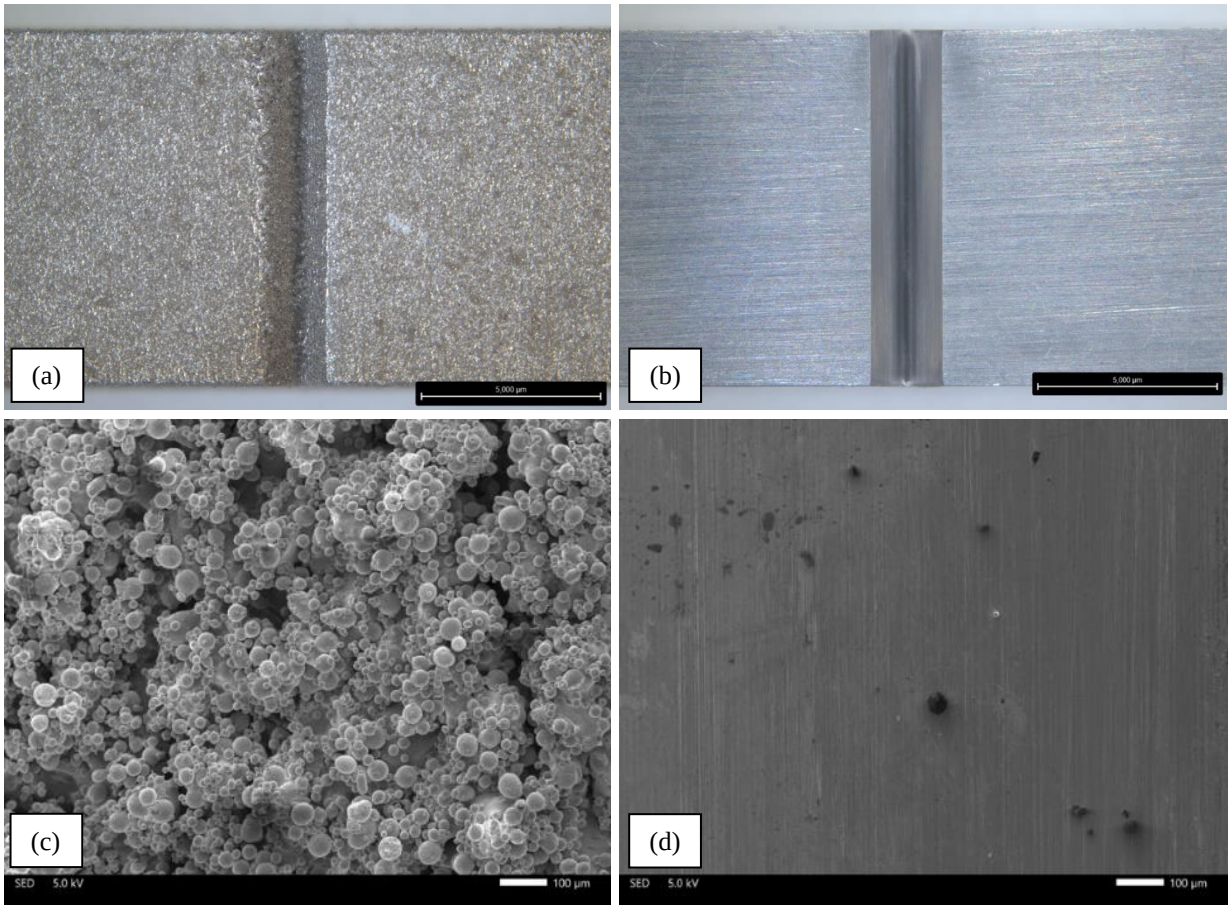

Figure 7. Top row images show the top face of the (a) printed notch Z bar and (b) machined notch bar. Bottom row SEM images show the interior surface of the notches of the (c) printed notch Z bar and (d) machined notch bar.

Surface roughness measurements were taken of the two types of specimens as shown in Table IV. The machined samples had an Ra below 1 µm, while the as-built sample had a higher roughness, 8.44 µm. ASTM E23 has a surface finish requirement for Ra (≤ 2 µm), so the printed notch Z bars did not meet this specification. Samples can be ground before testing to lower the surface roughness and reduce the wear on the anvils of the impact tester.

Table IV: Surface roughness measurements of impact bar samples.

Sample Type	Ra [µm]
Machined Notch	0.14
Printed Notch	8.44

Mechanical Testing

Figure 8 shows the individual impact energies of each bar tested. The heat treatments are ordered by the condition that reached the highest to the lowest impact energy. There was variation in the results of the individual machined bars and printed notch Z bars. Overall, the printed notch bars followed the same trend as the machined bars for the corresponding heat treatments. The printed notch bars showed typically a higher impact energy than the machined bars possibly due to the smaller notch depth than the machined notch bars as shown in Figure 6. The heat treatment that produced the highest impact energy was the austenitized (899 °C AC) samples. This condition produced the largest range of impact energies for the printed notch and machined samples as well. The as-built samples and intercritcally annealed (816 °C WQ) samples showed the next highest impact energies. The intercritically annealed (746 °C WQ) samples and the austenitized & intercritcally annealed samples (899 °C AC + 746 °C WQ) resulted in the lowest impact energy of the heat treatments. The deviation in the resulting impact energy between the machined and the printed notch bars could be due to the differences in notch geometry, overall dimensions and surface finish of the samples. However, the printed notch bars did show a strong correlation to the machined bars, so with further printing optimization or minimal post-processing a printed notch test sample could be used for preliminary benchmark testing to help decrease the cost and time of machining specimens.

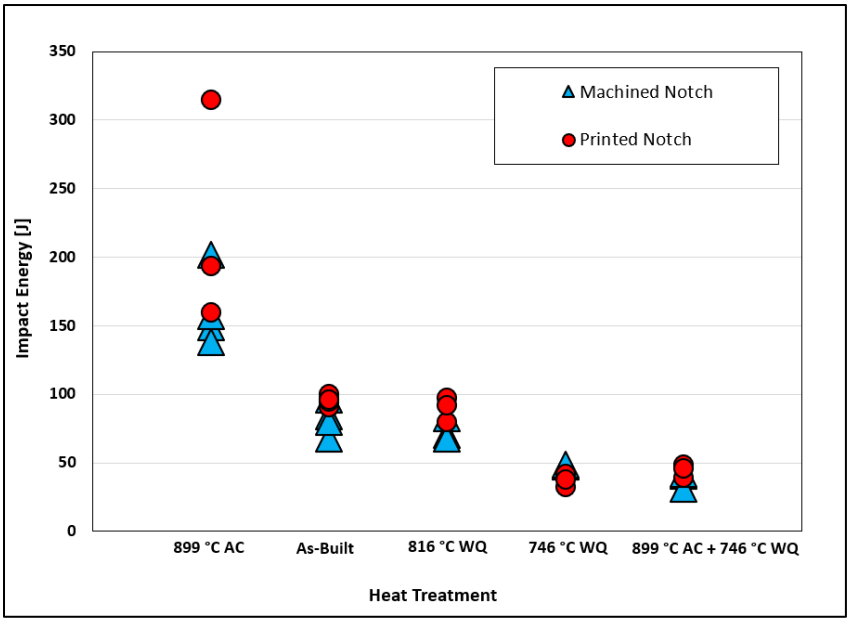

Figure 8. Impact energy of the machined and printed notch Z bars with different heat treatments.

In Figure 9 the average impact energy, yield strength, ultimate tensile strength, elongation, and hardness for each condition are plotted. The heat treatments are ordered in each graph by which condition produced the highest to lowest impact energy to examine the correlation to the other properties. The highest impact energy condition (899 °C AC) had the highest elongation, but the lowest ultimate tensile strength and hardness. The as-built condition had the next highest impact energy and also the highest yield strength, ultimate tensile strength and hardness. The intercritically annealed (816 °C WQ) heat treatment resulted in the closest properties to wrought DP600 and this condition had an average impact energy of 74 J. These properties can be further optimized to increase toughness while maintaining high strength levels by manipulating the microstructure.

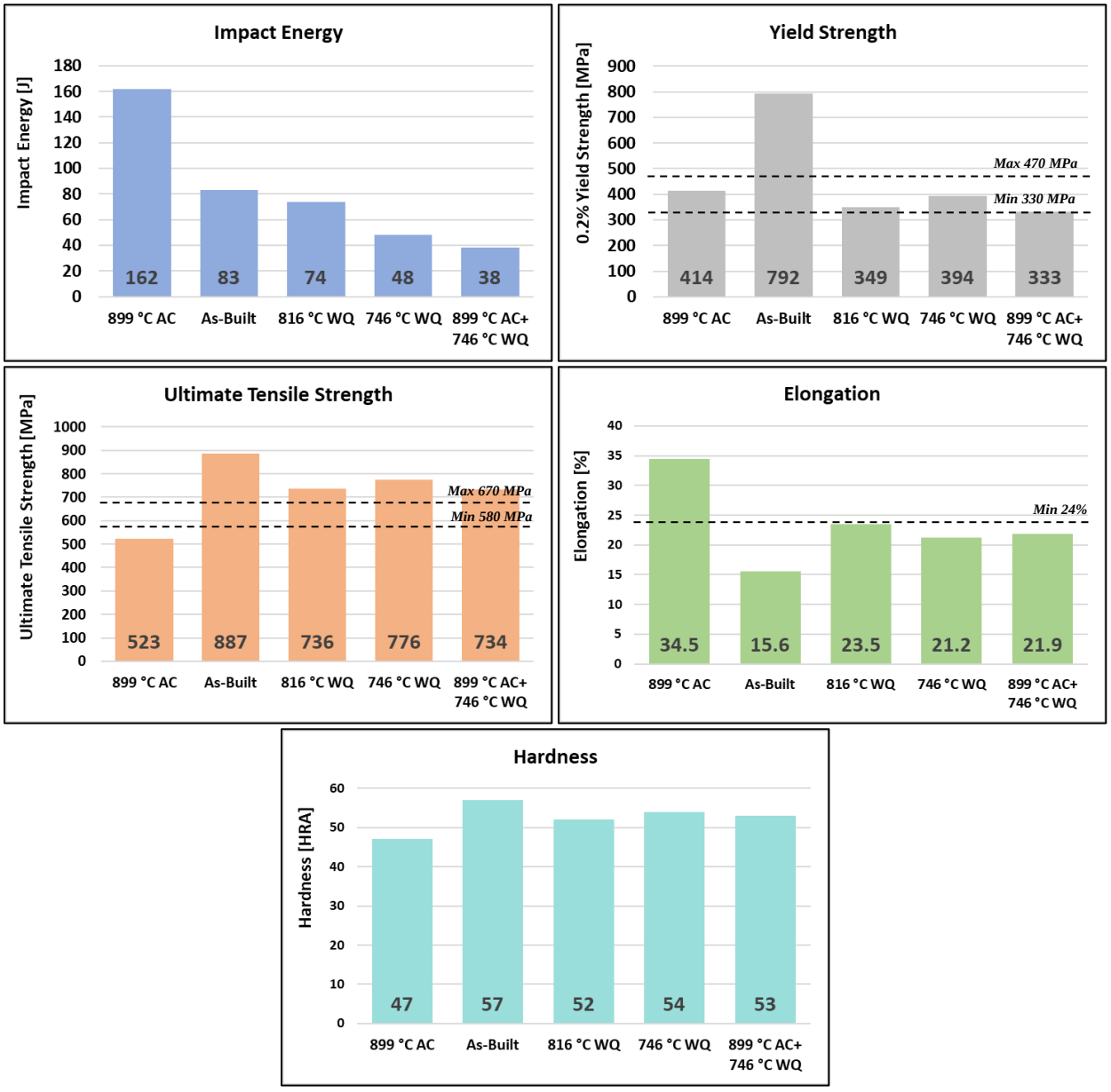

Figure 9. Graphs displaying the average properties of heat treated machined impact bars and tensile bars. The wrought DP600 mechanical properties specifications (Salzgitter) are shown on the graphs.[10]

Metallographic Analysis

Microstructural analysis was completed on the heat treated machined impact bars to observe the size, shape and distribution of phases present. The average impact energy of each condition is shown in the top left corner of each corresponding micrograph. The as-built microstructure shown in Figure 10 is composed of martenite, bainite, and ferrite. Overall the microstructure is very fine with low porosity levels. The grains show different sizes and shapes. This condition resulted in the second highest impact energy and also had the highest strength level.

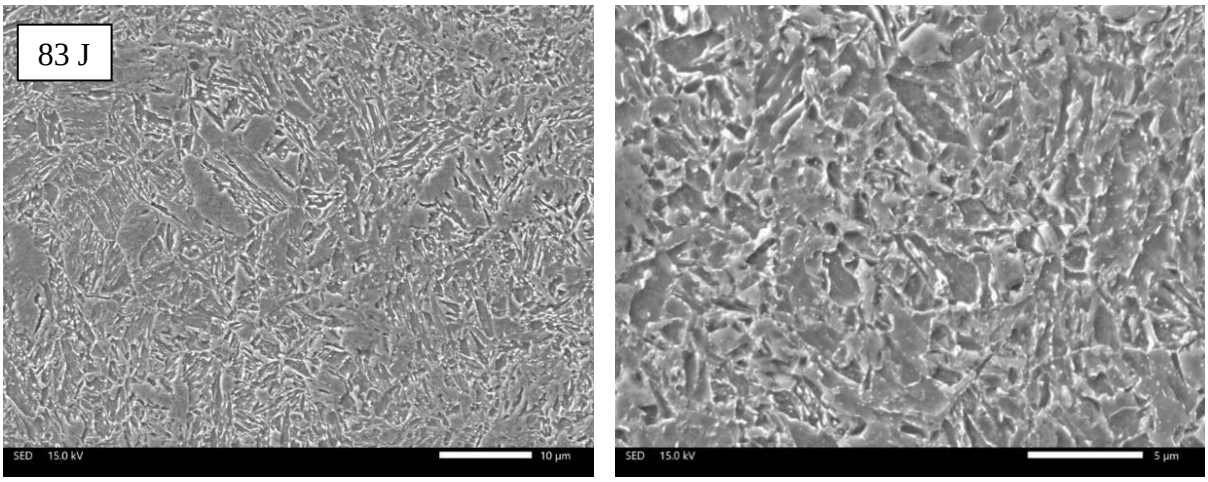

Figure 10. Microstructure of as-built impact bar. SEM

The microstructures of the heat treated samples are shown in Figure 11. The intercritically annealed (746 °C WQ) sample consisted of ferrite, bainite and martensite. Large grains of ferrite are present throughout the microstructure and have a non-uniform distribution. The microstructure of the samples that were intercritically annealed (816 °C WQ) contains ferrite and martensite. The ferrite grains have different sizes and shapes, but overall the microstructure is starting to appear more uniform than the lower temperature intercritical anneal condition. The microstructure of the austenitized (899 °C AC) samples contains a mixture of ferrite and pearlite. The ferrite grain size appears more uniform and is larger than the two intercritical annealing heat treatments. The microstucture of the last heat treatment where samples were austenitized and then intercritically annealed (899 °C AC + 746 °C WQ) is composed of ferrite, bainite and martensite. In this microstructure the transformation products are more isolated than the other intercritical annealing heat treatments. It is important to investigate the size, shape, and distribution of the second phase in DP steels because these characteristics will affect the mechanical properties.[3]

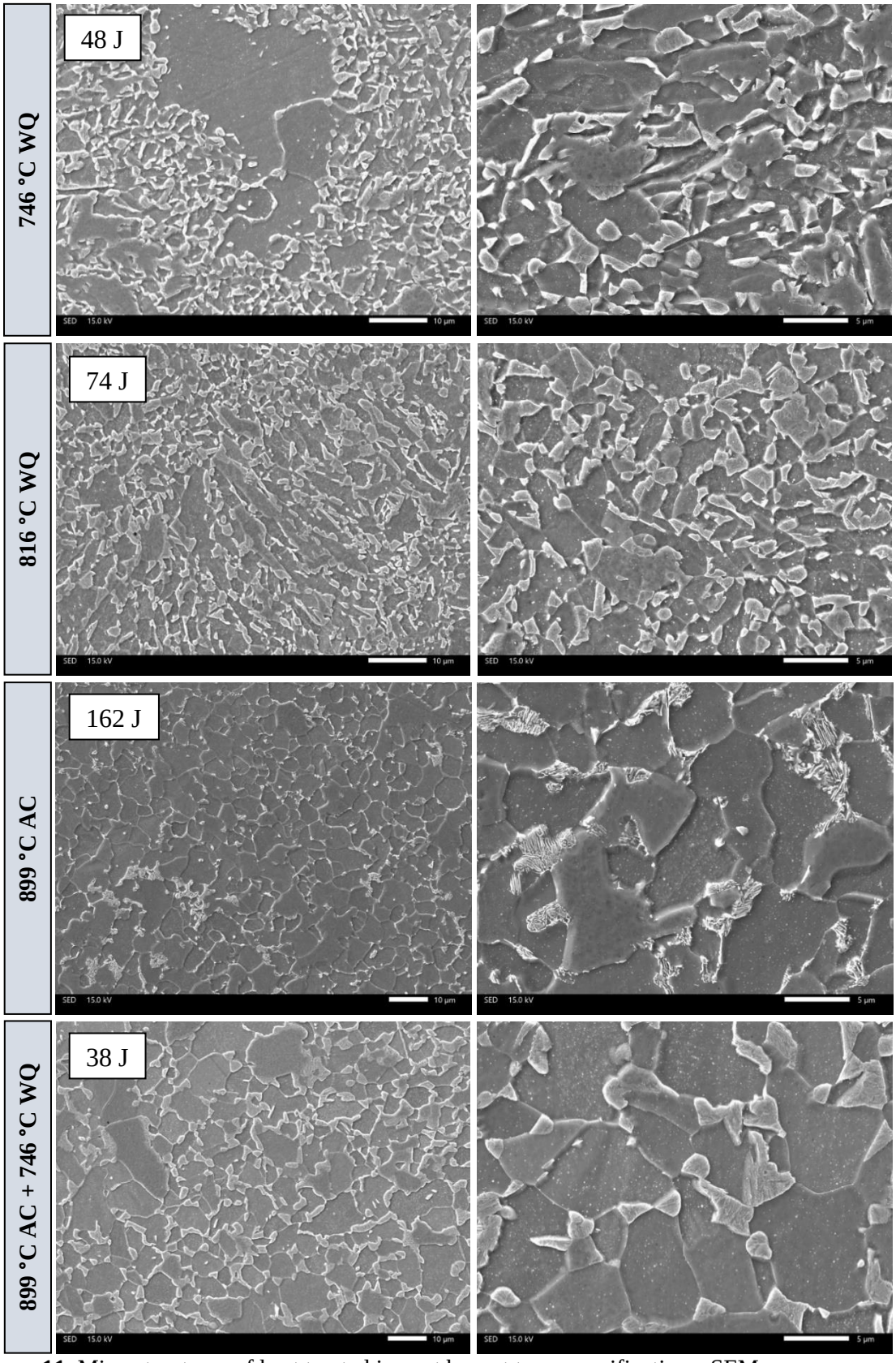

Figure 11. Microstructures of heat treated impact bars at two magnifications. SEM

The fracture surfaces of the machined impact bars were also examined by SEM. The average impact energy for each condition is shown in the top right corner of each corresponding micrograph. There are three mechanisms by which fracture can occur, clevage, intergranular and ductile failure, and it can also occur by a combination of these mechanisms.[9] Cleavage is a transgranular fracture mode that occurs along the crystallographic planes. Intergranular fracture occurs when cracks propagate along grain boundaries. When ductile failure occurs plastic deformation will precede fracture. During fracture voids are nucleated at inclusions, carbides or other dispersed phases and with increasing plastic strain these voids grow and coalesce resulting in a fracture surface covered in dimples.[9] Figure 12 shows the fracture surface of the as-built impact bar. This condition resulted in the second highest impact energy. Shear lips (jagged edges on left and right side of the bar) are observed as well as a high surface roughness indicative of ductile fracture. Ductile dimpling is observed in the SEM images as well as small oxides, which would decrease fracture toughness by promoting crack nucleation, void nucleation at the particle matrix interface and cause early coalescensce.[9]

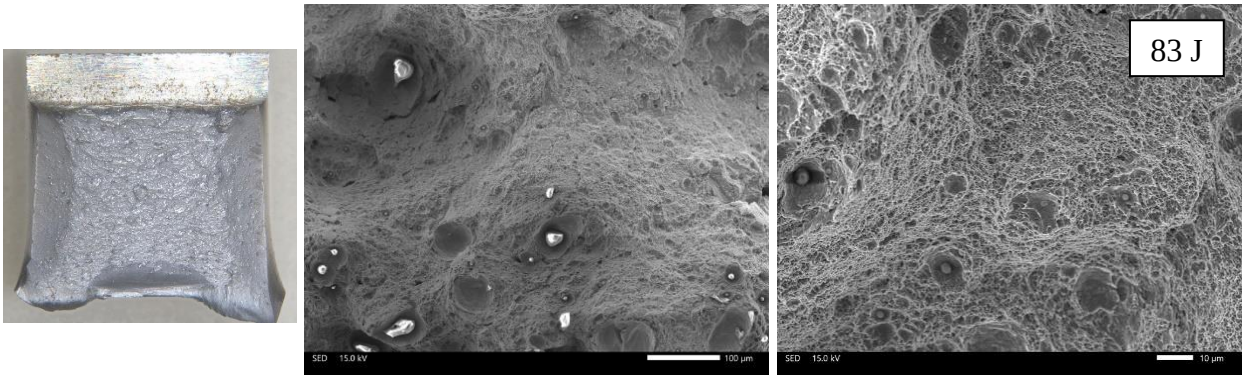

Figure 12. Fracture surface of the as-built impact bar. SEM

Figure 13 shows the fracture surfaces of the heat treated impact bars. The austenitized (899 °C AC) sample shows the most plastic deformation compared to the other conditions. The intercritical annealing heat treatments resulted in fracture surfaces that look more flat in appearance, which is indicative of a brittle failure or a mixture of failure modes. The intercritically annealed (816 °C WQ) sample shows shear lips on the sides of the bar and ductile dimpling is observed in the fracture surface. Less roughness is observed on this fracture surface as compared to the as-built and austenitized (899 °C AC) samples. The last two heat treatments resulted in the most brittle fractures of the group. They showed failure by combination of ductile rupture and brittle patches of cleavage. The intercritically annealed (746 °C WQ) sample shows large patches of cleavage surrounded by areas of ductile dimpling. The austenitized and intercritical annealed (899 °C AC + 746 °C WQ) samples show more areas of cleavage, but they are smaller in size.

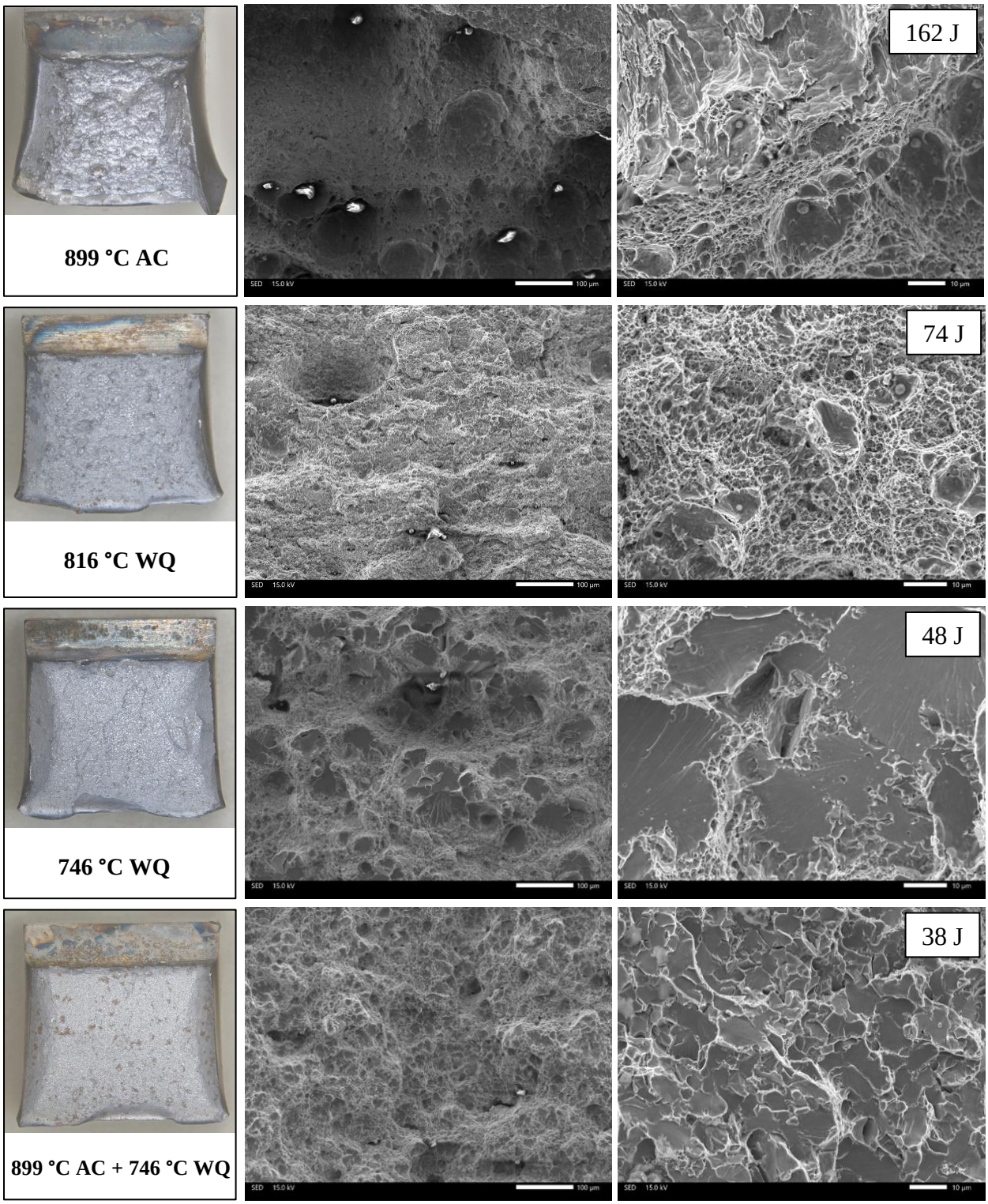

Figure 13. Fracture surfaces of heat treated impact bars. SEM

CONCLUSIONS

- Wrought DP600 grade steel was successfully printed using LPBF achieving comparable density and mechanical properties when using targeted heat treatments.
- The impact properties of printed Charpy V-notch bars were shown to correlate with machined notch bars (ASTM E23), however additional optimization of the printed notch testing sample is needed to be used for benchmark testing.
- Various heat treatments were evaluated to produce different microstructures and the influence on the resulting impact energy was shown.
- Laser printed DP600 steel can be heat treated to various combinations of strength, ductility, and toughness allowing one material to be utilized for multiple applications.

REFERENCES

1. F. C. Campbell. *Elements of Metallurgy and Engineering Alloys*. 2008, ASM International, Materials Park, Ohio.
2. R.A. Kot and B.l. Bramfit, *Fundamentals of Dual-Phase Steels*, 1981, The Metallurgical Society of AIME, Warrendale, Pa.
3. ASM Handbook Volume 9 Metallography and Microstructures, Published by ASM International, 2004.
4. Standard Guide for Additive Manufacturing-Design-Post-Processing Metal PBF-LB F3530-22, published by ASTM International.
5. K. Horvay, C. Schade, T. Murphy "Development of Dual Phase Steel for LPBF Application", *Proceedings of the PowdetMet 2021 Conference.*
6. Standard Test Methods for Notched Bar Impact Testing of Metallic Materials E23-18, published by ASTM International.
7. Standard Test Methods for Metal Powders and Powder Metallurgy Products, 2022, Metal Powder Industries Federation, Princeton, NJ.
8. ASM Handbook Volume 4 Heat Treating, Published by ASM International, 1991.
9. ASM Handbook Volume 19 Fatigue and Fracture, Published by ASM International, 2002.
10. DP600 Product Datasheet from Salzgitter Flachstahl, Edition 07/10 page 1.
11. A. Turnali, S. Motaman, Y. Chang, B. Bottger, A. Serafeim, L. Sayk, N. Peter, S. Richter, A. Schwedt, S. Hoges, C. Haase, "Evolution of Microstructural Heterogeneities in Additively Manufactured Low-Alloy Steel", Additive Manufacturing, 2023, vol. 78.